PAN ARCHIVES OF ACOUSTICS
Vol. 43, No. 2, pp. 163–175 (2018)

DOI: 10.24425/122364

Application of EMD ANN and DNN for Self-Aligning Bearing Fault Diagnosis

Narendiranath Babu T.[(1)], Arun ARAVIND[(1)], Abhishek RAKESH[(1)]
Mohamed JAHZAN[(1)], Rama Prabha D.[(2)]

[(1)] *School of Mechanical Engineering, VIT University*
Vellore, Tamil Nadu, India; e-mail: narendiranathbabu.t@vit.ac.in

[(2)] *School of Electrical Engineering, VIT University*
Vellore, Tamil Nadu, India

(*received June 14, 2017; accepted November 16, 2017*)

Self-aligning roller bearings are an integral part of the industrial machinery. The proper analysis and prediction of the various faults that may happen to the bearing beforehand contributes to an increase in the working life of the bearing. This study aims at developing a novel method for the analysis of the various faults in self-aligning bearings as well as the automatic classification of faults using artificial neural network (ANN) and deep neural network (DNN). The vibration data is collected for six different faults as well as for the healthy bearing. Empirical mode decomposition (EMD) followed by Hilbert Huang transform is used to extract instantaneous frequency peaks which are used for fault analysis. Time domain and time-frequency domain features are then extracted which are used to implement the neural networks through the pattern recognition tool in MATLAB. A comparative study of the outputs from the two neural networks is also performed. From the confusion matrix, the efficiency of the ANN has been found to be 95.7% and using DNN has been found to be 100%.

Keywords: self-aligning bearing; fault classification; artificial neural networks; deep neural networks.

1. Introduction

Self-aligning bearings consist of two ball rows attached to a common raceway. They align themselves in order to accommodate for any misalignment. Hence their application mainly comes where misalignment occurs due to problems in mounting or deflection in shaft. They are commonly used in plummer block units, conveyor belts, and blowers.

Under the working condition of the bearing, the friction generated in them is low and this enables them to operate at cooler temperatures even at high speed working conditions. Since the heat generation is low, this makes temperature of bearing lower leading thus to a longer bearing life.

As self-aligning bearings are a common part of machinery in industry, monitoring the condition of bearing is a serious issue. The vibrations emitted by bearing parts are key in analysis of the faults. Thus collection of sensitive data is also important. The common faults getting induced on bearing are cracks, wear defect, and looseness of balls.

In this paper vibration analysis is done on six different faults induced on self-aligning bearing. The first fault is a wear defect in the inner surface of the inner race. This is generated usually due to improper fits or due to excess load. The second fault is damage in the circumference of the inner race. The third, fourth, and fifth faults are due to looseness in one, two, and three balls from the self-aligning bearing, respectively.

Huang *et al.* (1998) investigated the empirical mode decomposition and the Hilbert spectrum for non-linear and non-stationary time series analysis. The authors deal with decomposing any data set into a number of intrinsic mode functions by the empirical mode decomposition method, and these intrinsic mode functions admit well-behaved Hilbert transforms. This methodology has been adopted for analysing the vibration data of self-aligning bearings.

Wu *et al.* (2016) investigated the defect diagnosis of journal bearings using instantaneous frequency normalisation under fluctuant rotating speed. Here, the empirical mode decomposition method as well as the instantaneous frequency calculation are used to

construct the time-frequency domain of the envelope signals of the vibration data. The magnitude distributions of the envelope spectrum at the corresponding bearing defect related frequencies were extracted as the feature vectors. The support vector machine was then used to classify the extracted feature vectors of the different bearing fault cases. This study focuses on defect analysis of self-aligning bearings at constant rotating speeds and no load conditions.

Feng *et al.* (2016) investigated the amplitude-frequency demodulation analysis for fault diagnosis of planetary bearings. By first decomposing the signal into intrinsic mode functions (IMFs) using empirical mode decomposition (EMD), the mono-component need of instantaneous frequency is satisfied. Further frequency demodulation analysis is performed on a sensitive component with instantaneous frequency within the resonance frequency. The peaks are matched to find the planet bearing fault. In the study, the authors deal with various components of planetary bearings and similar analysis needs to be worked out for self-aligning bearings.

Boashash (1992a; 1992b) investigated the methods of estimating and interpreting the instantaneous frequency of the signal. Decomposition of non-stationary signals is difficult in sinusoidal components. In such signals, the idea of frequency is not effective, and there arises the need to use a term which accounts for the time-varying nature of the process. In this study, the instantaneous frequency of the decomposed signal is used for estimating the fault condition of the self-aligning bearing.

Ibrahim *et al.* (2008) devised methods to estimate the instantaneous frequency for diagnosis of faults in induction machines. In the paper, the idea of instantaneous frequency is exploited to find information related to the defect. The authors deal with defects in induction machines and similar principles were adopted in the current study also.

Huang *et al.* (1999) utilised the Hilbert spectrum for the analysis of non-linear water waves. It highlighted the advantages of Hilbert spectrum over fast Fourier transform and wavelet spectral analysis. Through Hilbert spectral analysis, the variation of signal with time can be calculated. As compared to wavelet, it is able to give improved resolution of time-frequency.

Yang (2008) published a paper on the methods of interpretation of data signals using an improved Hilbert-Huang transform. Most of the intrinsic mode functions are multi-harmonic functions which give irregular frequencies. The improved Hilbert Huang transform can make up for this irregularity. These concepts are used in the study of the analysis of different faults in self-aligning bearing.

Rato *et al.* (2008) investigated some of the problems of HHT and their solution. This paper analyses various drawbacks of EMD and the methods to overcome it. Various sifting stopping criteria have been tested to get the best IMFs. The paper incorporates certain parameters like energy ratio which can suitably modify the final obtained output.

Samanta *et al.* (2003) compared artificial neural networks with support vector machines for bearing fault classification. Here, time-domain vibration signals were used for feature extraction, which was used to train the network. The method highlighted on the efficiency of artificial neural networks for feature extraction with neural networks.

Ali *et al.* (2015) investigated the automatic fault diagnosis of bearings and classification of faults using vibration signals based on the empirical mode decomposition and Artificial neural networks. This feature extraction method uses empirical mode decomposition and mathematical analysis of the measured data in order to select the most significant intrinsic mode functions. The feature extraction method was used to extract eighteen different features which were used for pattern recognition in ANN and DNN.

Gan, Wang (2001) constructed a hierarchical diagnosis network based on deep learning and its application in the fault recognition pattern of journal bearings. The network uses two similar ones constructed by support vector machine and back propagation neural network. The study highlights on the efficiency of the hierarchical deep network.

Vyas, Satishkumar (2001) used artificial neural networks for fault identification and classification in a rotor-bearing system. Statistical moments were calculated for the vibration signals which were used to train the network. The current study focuses on training the network using data obtained from feature extraction which enabled producing more accurate results.

Saridakis *et al.* (2008) used artificial neural networks for measurements of various journal bearing performance parameters. A fault diagnosis model was created that uses ANN to identify the effects of increase in wear depth and increment of the misalignment angle in journal bearings. The methodology was utilised in analysing the various faults in self-aligning bearings studied in the current research.

Kim, Valdés (2003) developed a non-linear model for forecasting droughts by combining wavelet transforms and neural networks. The work highlights the efficiency of the method for correct predictions for non-linear and non-stationary data. However, in the current study, empirical mode decomposition was used for feature extraction of journal bearing vibration data.

Chen *et al.* (2017) investigated the rolling bearing fault diagnosis using deep neural networks. In the study, three different deep neural network models were employed for fault analysis of roller bearing. The accuracy in DNN method over ANN was studied.

Jia *et al.* (2016) investigated the intelligent fault diagnosis of rotating machinery with massive data. This paper points on the advantages of using deep neural networks over shallow networks. The effectiveness of this method is further validated using data from rolling element bearing and planetary gearboxes. This idea has been used for self-aligning bearings in the present study.

2. Experimental procedure

The vibration data of self-aligning bearing was collected using a whirling shaft apparatus. The 8 mm diameter shaft was operated at a speed of 1100 rpm. The apparatus used is shown in Fig. 1 below.

Fig. 1. Apparatus for measuring the bearing vibration data.

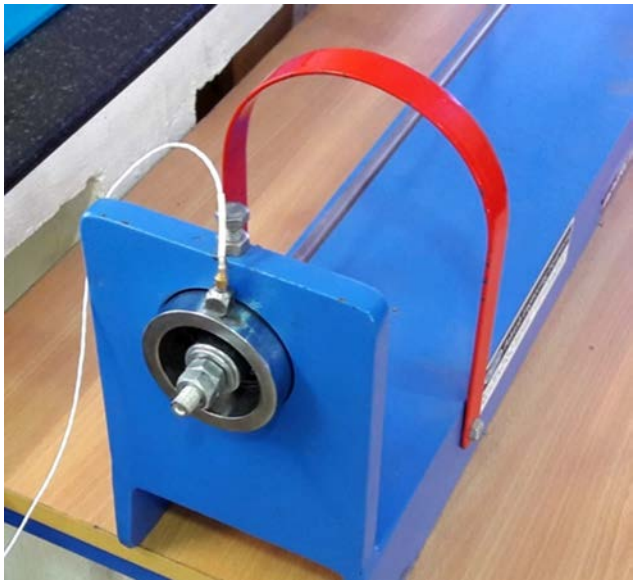

Fig. 2. Attachment of sensor to bearing housing.

In self-aligning bearings, six different fault conditions have been induced. Vibration data have been collected for each of these six faults as well as the healthy bearing shown in Fig. 3a. For the first fault, a stone-grinder was employed to create a wear defect in the inner surface of the inner race, as shown in Fig. 3b. For the second fault, the circumference of the cage was damaged using the stone grinder as shown in Fig. 3c. The third, fourth, and fifth faults were induced by respectively removing one, two, and three balls from the self-aligning bearing. The sixth fault was induced by making a wear defect on the inner surface of the outer race, as shown in Fig. 3d.

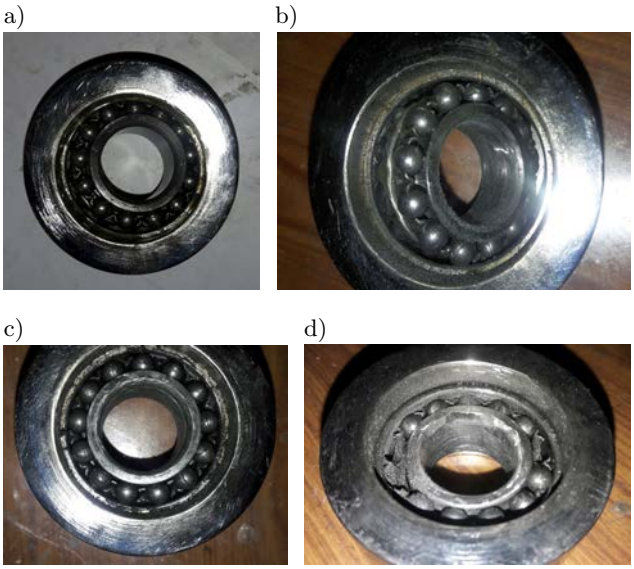

Fig. 3. a) Healthy self-aligning bearing, b) self-aligning bearing with fault 1 induced, c) self-aligning bearing with fault 2 induced, d) self-aligning bearing with fault 3 induced.

3. Methodology

3.1. Empirical mode decomposition (EMD)

The EMD method is performed on the obtained vibration data using the intrinsic mode functions (IMFs). EMD is a self-adaptive signal processing method that may be used for the analysis of both non-linear and non-stationary data. The EMD method is based on the local characteristic time scale of the signal and is capable of breaking down the signal into a finite number of intrinsic mode functions. The following algorithm was employed for performing the empirical mode decomposition of the experimentally obtained data:

(i) Original signal for five seconds is taken as $x(t)$.

(ii) All maxima and minima of the original signal are determined and joined using cubic interpolation. This produces an upper and a lower envelope.

(iii) The average of theses upper and lower envelopes is calculated for each data point.

(iv) This average is then subtracted from the original signal to obtain a new signal say, $x_1(t)$.

(v) Then, $x_1(t)$ is checked for the two IMF conditions – (a) the difference between the number of maxima/minima and number of zero crossings must be either zero or one and (b) the local average of the envelopes must be zero.

(vi) If $x_1(t)$ meets the above condition, $x(t)$ is replaced with the residual, IMF$\{1\}(t)$, where IMF$\{1\}(t) = x(t) - x_1(t)$.

(vii) If the above condition is not satisfied, $x(t)$ is replaced by $x_1(t)$.

(viii) The above conditions are repeated until we receive a monotonic residual.

3.2. Application of Hilbert Huang transform (HHT)

Once the intrinsic mode function components are obtained, the Hilbert transform is applied to each component to calculate the instantaneous frequency. Hilbert spectral analysis is used for obtaining the peaks for instantaneous frequency. Faults can be analysed by matching these peaks with the known data. The following algorithm is performed to incorporate HHT.

(i) The signal is taken as $x(t)$.

(ii) IMF$\{1\}$ to IMF$\{4\}$ is determined (for calculation purpose).

(iii) Let $a =$ IMF$\{1\}$ for the complete array of values.

(iv) Hilbert transform on a yields a complex number – $a + ib$ where b is the Hilbert transform of a.

(v) Phase

$$\varphi = \tan^{-1}\left(\frac{b}{a}\right). \tag{1}$$

(vi) Instantaneous amplitude

$$A = \sqrt{a^2 + b^2}. \tag{2}$$

(vii) Instantaneous frequency

$$\omega = \frac{\mathrm{d}\varphi}{\mathrm{d}t} \tag{3}$$

3.3. Automatic fault classification using ANN

Automatic classification of the faults in self-aligning bearing is done using artificial neural networks. They make it possible to continuously monitor the bearing condition and evaluate the severity of the defect online. ANN is widely considered as an effective tool for assessing the performance degradation of the bearing without human involvement.

The vibration signal data of the self-aligning bearing in the healthy condition and for each of the three different fault conditions for 120 seconds are collected. The initial 20% data for each second are collected and stored as a two-dimensional array. The initial step comprises extracting the time domain and time-frequency domain features. Feature extraction is mainly employed to assess the bearing performance degradation over time. An increase in bearing degradation is indicated by an increase in the magnitude of time domain features. Time domain features include eight classical features – RMS, kurtosis, skewness, peak to peak, crest factor, shape factor, impulse factor, margin factor – and two new features – add factor 1 and add factor 2. These two new features are used to link different features together. All these ten factors are summarised in Eqs. (4) to (13). In the equations, the value of init is calculated as the average of RMS of the healthy self-aligning bearing.

$$\mathrm{RMS} = \left(\frac{1}{N}\sum_{i=1}^{N} x_i^2\right)^{1/2}, \tag{4}$$

$$\mathrm{Kurtosis} = \frac{1}{N}\sum_{i=1}^{N}\frac{(x_i - \overline{x})^4}{\sigma^4}, \tag{5}$$

$$\mathrm{Skewness} = \frac{1}{N}\sum_{i=1}^{N}\frac{(x_i - \overline{x})^3}{\sigma^3}, \tag{6}$$

$$\text{Peak to peak} = x_{\max} - x_{\min}, \tag{7}$$

$$\text{Crest Factor} = \frac{\max|x_i|}{\mathrm{RMS}}, \tag{8}$$

$$\text{Shape Factor} = \frac{\mathrm{RMS}}{\frac{1}{N}\sum\limits_{i=1}^{N}|x_i|}, \tag{9}$$

$$\text{Impulse Factor} = \frac{\max|x_i|}{\frac{1}{N}\sum\limits_{i=1}^{N}|x_i|}, \tag{10}$$

$$\text{Margin Factor} = \frac{\max|x_i|}{\left(\frac{1}{N}\sum\limits_{i=1}^{N}|x_i|^{1/2}\right)^2}, \tag{11}$$

$$\text{Add Factor 1} = \log\left(\mathrm{Kurtosis} + \frac{\mathrm{RMS}}{\mathrm{Init}}\right), \tag{12}$$

$$\text{Add Factor 2} = \log\left(\mathrm{Kurtosis}^{(\text{Crest Factor})} + \left(\frac{\mathrm{RMS}}{\mathrm{Init}}\right)^{(P\_P)}\right). \tag{13}$$

Other than the ten time domain features obtained above, EMD is used to extract a set of new features called time-frequency domain values to make up for a more reliable database of features. Here, the bearing vibration signal is decomposed into characteristic IMFs. In the study, only the first seven IMFs are considered. The total energy of all the IMFs are calculated as:

$$E = \sum_{i=1}^{n} E_i. \tag{14}$$

A feature vector is calculated as:

$$[\mathrm{Ent},\ E_1/E,\ E_2/E,\ \ldots,\ E_7/E] = [\mathrm{Ent},\ \mathrm{EntIMF1},\ \mathrm{EntIMF2},\ \ldots,\ \mathrm{EntIMF7}], \tag{15}$$

where

$$\mathrm{Ent} = \sum_{i=1}^{n} P_i \log P_i. \tag{16}$$

Taking 120 samples from each of the six different available cases, the output is linked to a 4×720 matrix. This output is modelled using the pattern recognition tool in MATLAB – nprtool – which uses the 18 extracted features as inputs and 10 hidden neurons to give the output by scaled conjugate gradient method of training. 70% of the available data were employed for training, 15% data for validation, and 15% data were used for testing the neural network. The neural network performance was analysed using the cross entropy technique. The error histogram, confusion matrix, and receiver operating characteristics (ROC) plots have been used to analyse the performance of the created neural network.

3.4. Automatic fault classification using DNN

A deep learning network may be described as a group of artificial neural networks stacked together one after the other. In this research, an autoencoder has been used for realisation of deep neural networks. Also referred to as a Diabolo network, it is a feed-forward, non-recurrent network having an input layer, an output layer, and one or more hidden layers connecting them. Here, for the vibrational data, an autoencoder with a hidden layer size of 10 and a linear transfer function is trained for the decoder. The features are extracted in the hidden layer for the first autoencoder, and these features are used to train a second autoencoder. Features are again extracted in the hidden layer for the second autoencoder. These features are then used to train a softmax layer for classification. The deep neural network is formed by stacking the encoders together with the softmax layer. The deep network is trained based on these obtained data and the network performance is measured with the aid of a confusion matrix.

4. Results and discussion

4.1. Collection of vibration data and empirical mode decomposition

The vibration data collected from the experimental setup of the self-aligning bearing have been utilised to perform the empirical mode decomposition and Hilbert-Huang transform to obtain the Hilbert-Huang spectrum as in the case of the journal bearings. The intrinsic mode functions are obtained, and the various peaks obtained are used to compare the various faults.

In the current study, a self-aligning roller bearing with bearing number 2205 was used. Substituting the values in the frequencies, we get:

- natural frequency of vibration $= 1100/60 = 18.33$ Hz,
- fundamental train frequency,
$$\text{FTF} = \frac{S}{2}\left(1 - \frac{B_d}{P_d}\cos\Phi\right) = 7.5153 \text{ Hz},$$
- inner ring ball pass frequency,
$$\text{BPFI} = \frac{N_b}{2}\left(1 + \frac{B_d}{P_d}\cos\Phi\right) = 140.2245 \text{ Hz},$$
- outer ring ball pass frequency,
$$\text{BPFO} = \frac{N_b}{2}S\left(1 + \frac{B_d}{P_d}\cos\Phi\right) = 98.0655 \text{ Hz},$$
- ball spin frequency,
$$\text{BSF} = \frac{P_d}{2B_d}S\left[1 - \left(\frac{B_d}{P_d}\right)^2(\cos\Phi)^2\right] = 48.5745 \text{ Hz},$$

where S means revolutions per second $=18.33$ Hz, B_d is the ball diameter $= 7.13$ mm, N_b is the number of balls $= 13$, P_d is the pitch diameter $= 38.98$ mm, Φ is the contact angle $=15°$.

The fault induced on each part of the self-aligning bearing produces a corresponding frequency spike on the same frequency as the natural frequency of the part where the fault was induced.

4.2. Self-aligning bearing at healthy condition

This corresponds to the normal operation of a healthy self-aligning bearing shown in Fig. 3a. The shaft rotates in the healthy bearing with sufficient lubrication and hence the vibrations produced would be much fewer. From Fig. 4c, in this case, a peak amplitude of 0.01471 m/s^2 and frequency of 18.47 are obtained.

4.3. Self-aligning bearing at fault 1 condition

This corresponds to the operation of a self-aligning bearing at fault 1 condition, as shown in Fig. 3b. In this case, the inner surface of the inner race of the bearing has been subjected to wear damage using a stone grinder, thereby increasing the friction between the bearing and the shaft. From Fig. 5c, in this case, a peak amplitude of 0.2473 m/s^2 and a frequency of 140.3 Hz are obtained.

4.4. Self-aligning bearing at fault 2 condition

This corresponds to the operation of a self-aligning bearing at fault 2 condition, as shown in Fig. 3c. In this case, the circumference of the cage of the bearing has been subjected to wear damage using a stone grinder, thereby causing improper fit of the shaft in the bearing. From Fig. 6c, in this case, a peak amplitude of 0.4217 m/s^2 and frequency of 140.2 Hz are obtained.

4.5. Self-aligning bearing at fault 3 condition

This corresponds to the operation of a self-aligning bearing at fault 3. In this case, a single ball is removed from the cage of the ball bearing, and the bearing is made to run while the vibration measurements are taken. From Fig. 7, in this case, a peak amplitude of 0.0610 m/s^2 and frequency of 8.223 Hz are obtained. The fundamental train frequency has been noted in this case.

a)

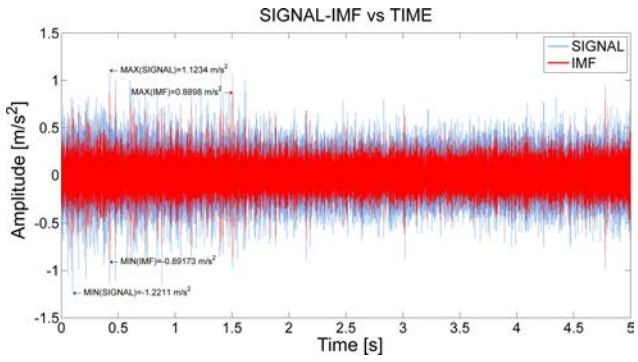

b)

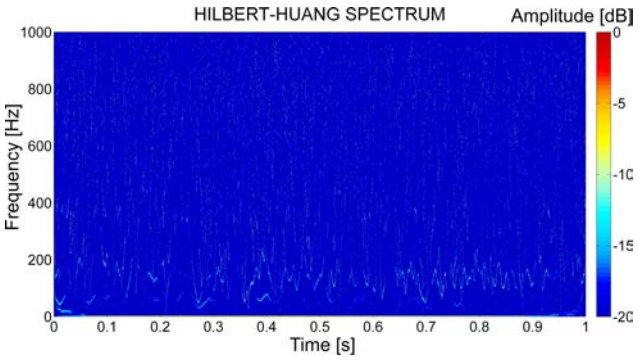

c)

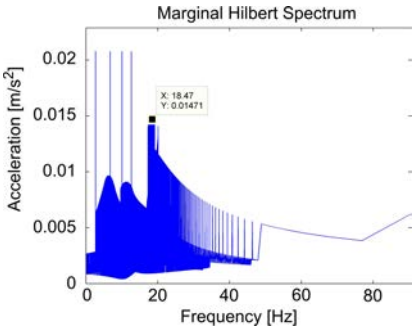

Fig. 4. a) Original signal with IMFs, b) Hilbert-Huang spectrum, c) marginal Hilbert spectrum for healthy self-aligning bearing.

a)

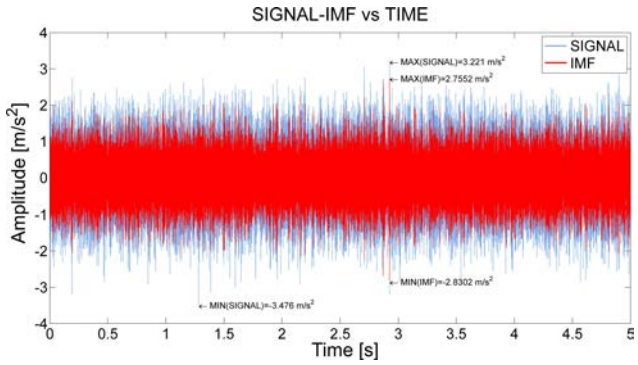

b)

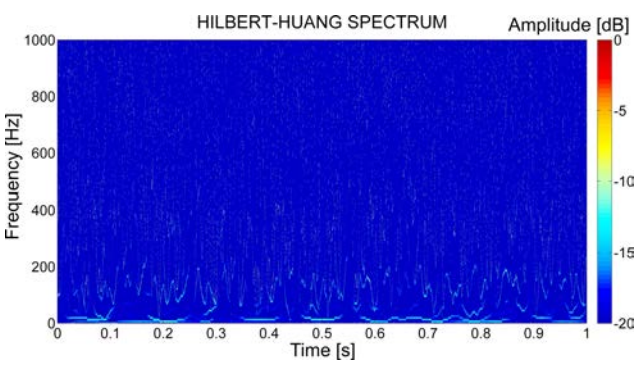

c)

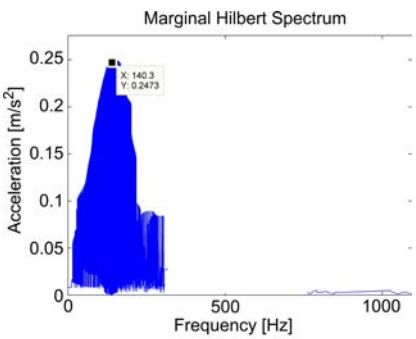

Fig. 5. a) Original signal with IMFs, b) Hilbert-Huang spectrum, c) marginal Hilbert spectrum for fault 1 condition of self-aligning bearing.

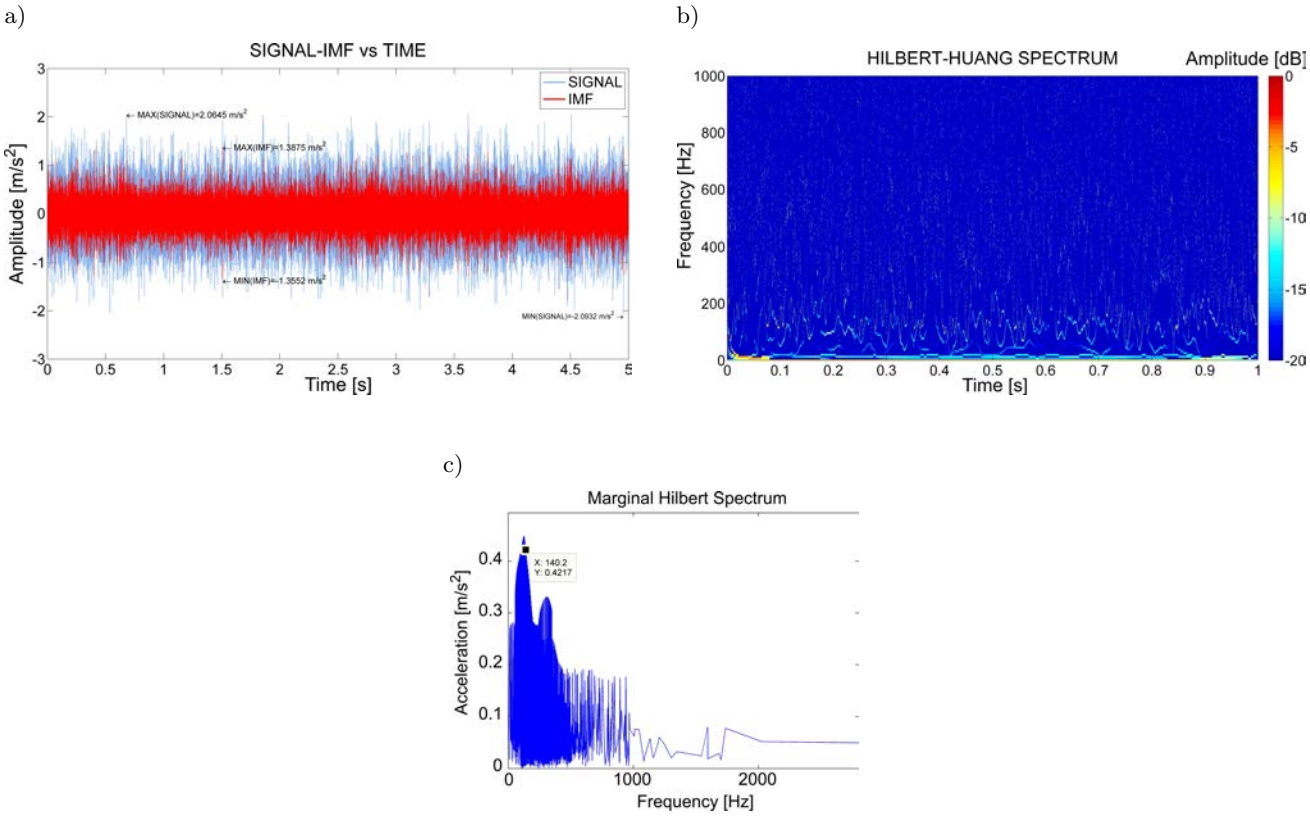

Fig. 6. a) Original signal with IMFs, b) Hilbert-Huang spectrum, c) marginal Hilbert spectrum for fault 2 condition of self-aligning bearing.

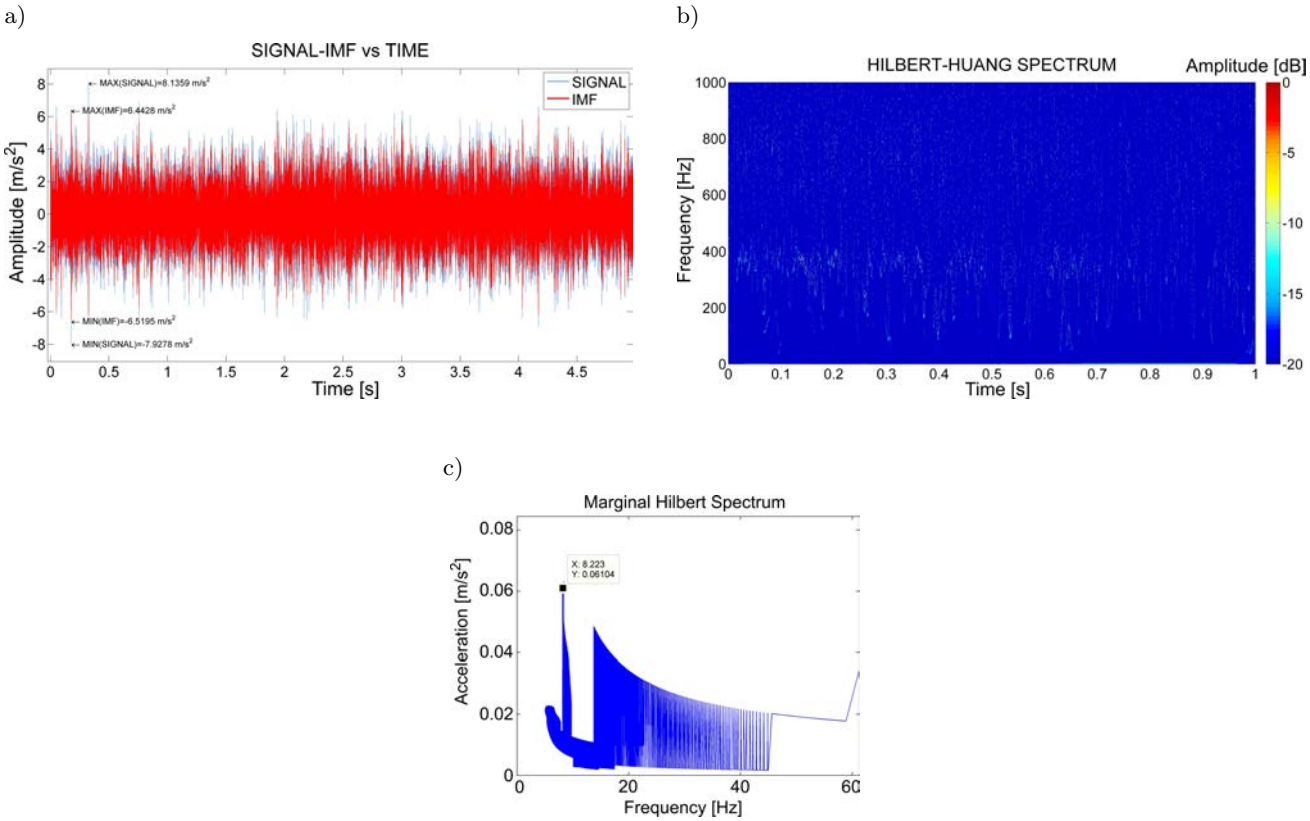

Fig. 7. a) Original signal with IMFs, b) Hilbert-Huang spectrum, c) marginal Hilbert spectrum for fault 1 condition.

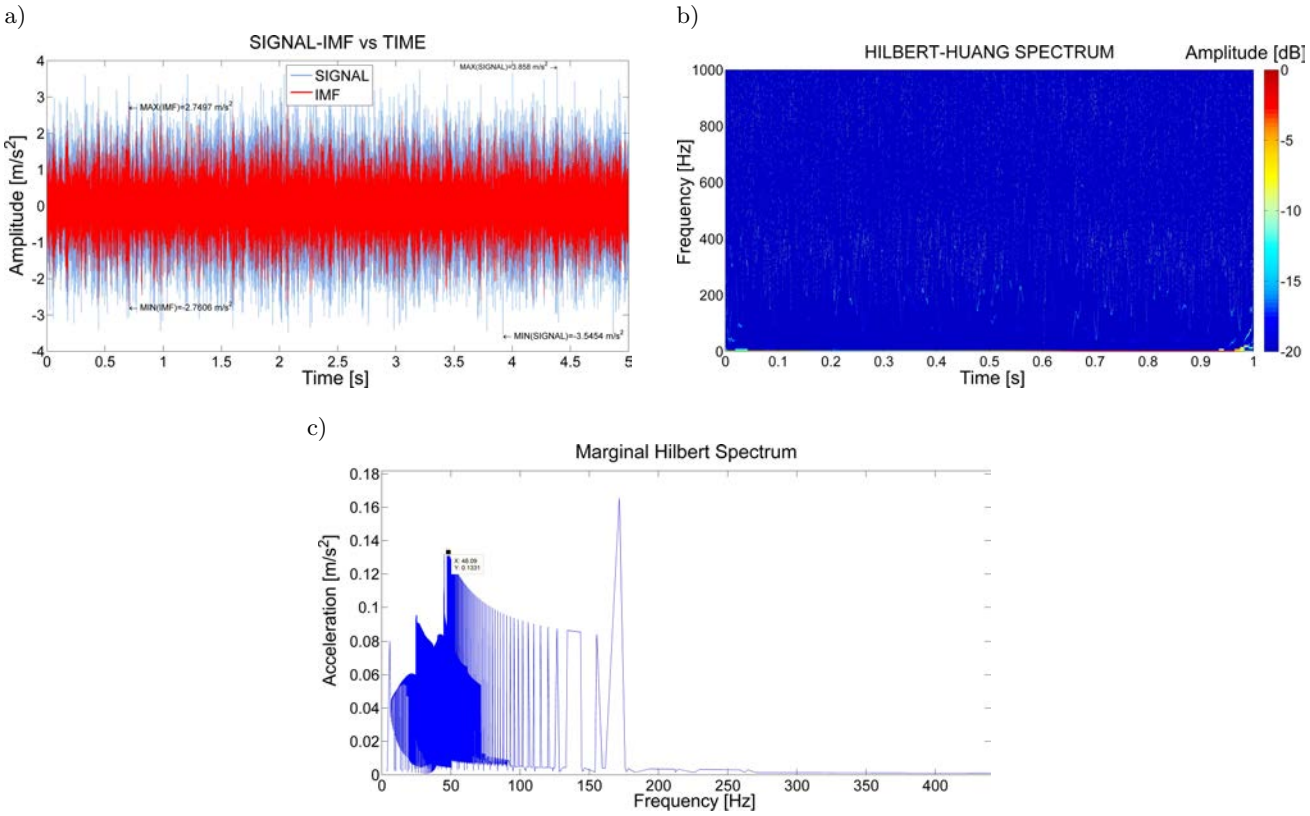

Fig. 8. a) Original signal with IMFs, b) Hilbert-Huang spectrum, c) marginal Hilbert spectrum for fault 4 condition.

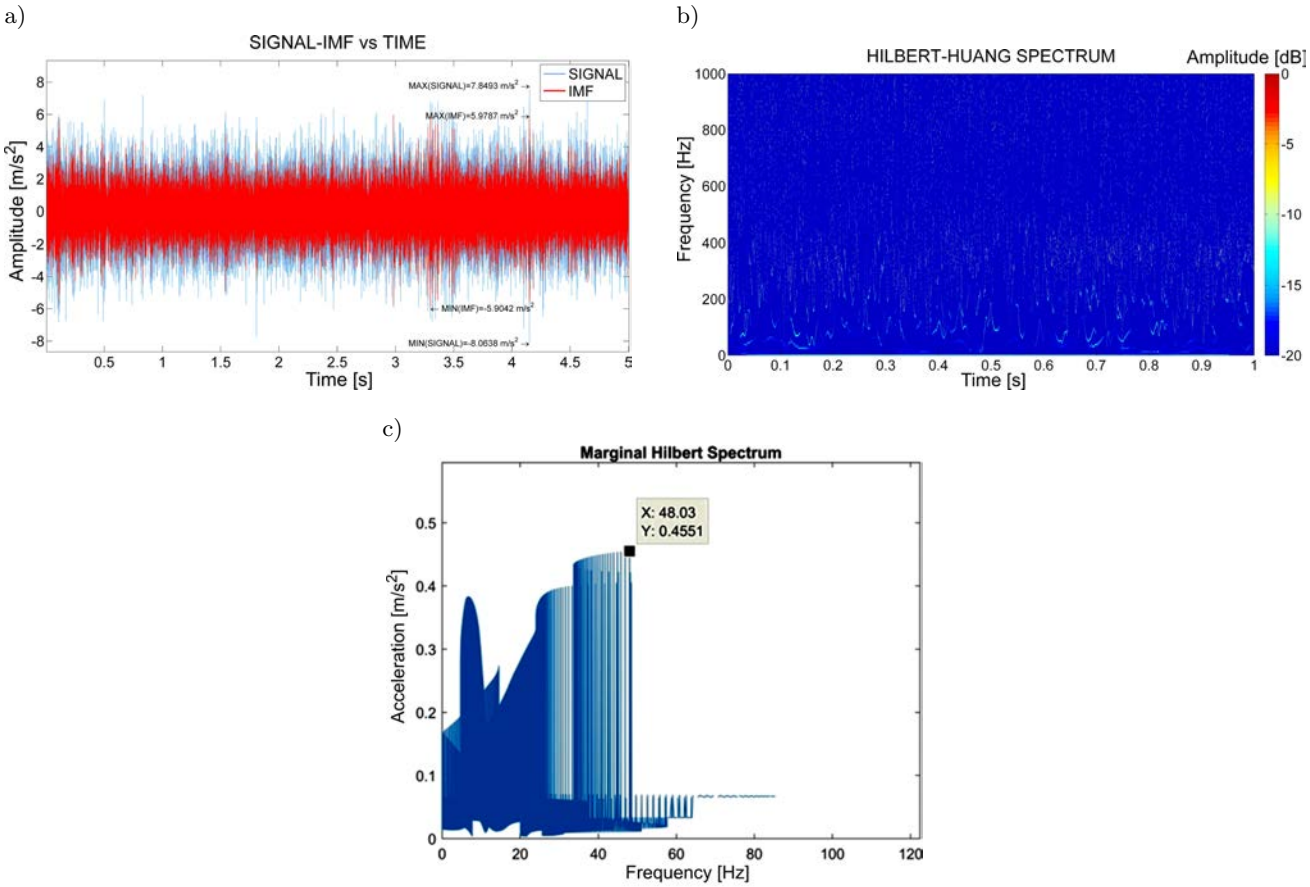

Fig. 9. a) Original signal with IMFs, b) Hilbert-Huang spectrum, c) marginal Hilbert spectrum for fault 5 condition.

4.6. Self-aligning bearing at fault 4 condition

This corresponds to the operation of a self-aligning bearing at fault 4. In this case, two balls are removed from the cage of the ball bearing and the bearing is made to run while the vibration measurements are taken. From Fig. 8c, in this case, a peak amplitude of 0.1331 m/s^2 and frequency of 48.09 Hz are obtained.

4.7. Self-aligning bearing at fault 5 condition

This corresponds to the operation of a self-aligning bearing at fault 5. In this case, three balls are removed from the cage of the ball bearing and the bearing is made to run while the vibration measurements are taken. From Fig. 9c, in this case, a peak amplitude of 0.4551 m/s^2 and frequency of 48.03 Hz are obtained.

4.8. Self-aligning bearing at fault 6 condition

This corresponds to the operation of a self-aligning bearing at fault 6 condition as shown in Fig. 3d. In this case, the inner surface of the outer race of the bearing has been subjected to wear damage using a stone grinder, thereby reducing the proper fit between the housing and the bearing. From Fig. 10c, in this case, a peak amplitude of 0.5699 m/s^2 and frequency of 97.94 Hz are obtained.

4.9. Automatic fault classification using artificial neural networks (ANN)

ANN implementation has been performed on the no load condition of various fault conditions with different criteria. Scaled conjugate gradient method has been used for training with 10 hidden neurons. 70% of the available data have been used for training, 15% of the data have been used for validation, and the remaining 15% have been used for testing. The confusion matrix, receiver operating characteristics plot, performance diagram, and training state performance have been plotted for the same. From the confusion matrix, the efficiency of the neural network has been found to be 95.7%. 18 different features, six different faults, and the healthy bearing are given as inputs.

a)

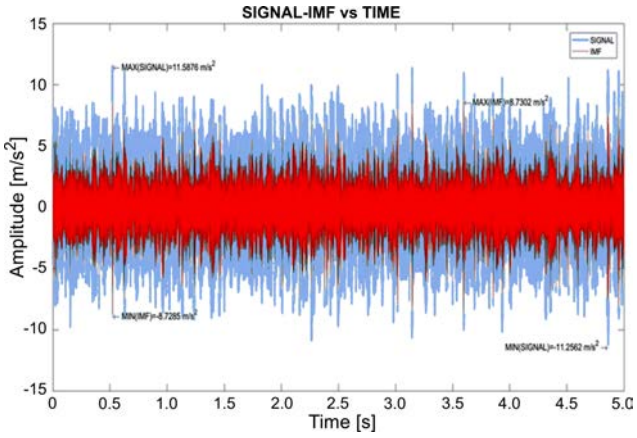

b)

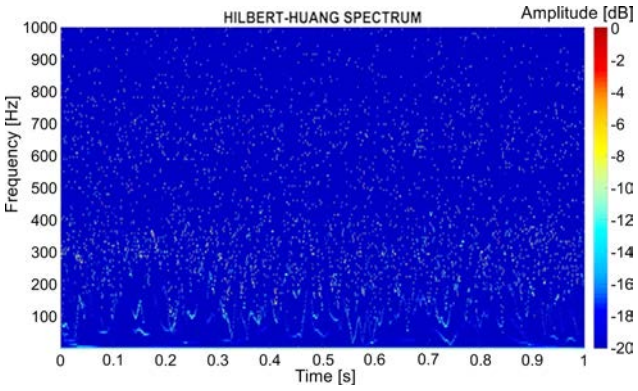

c)

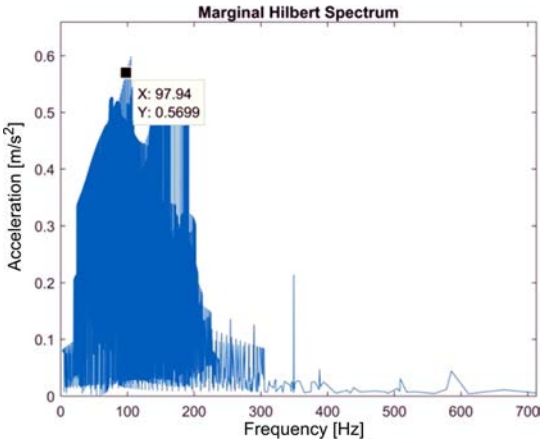

Fig. 10. a) Original signal with IMFs, b) Hilbert-Huang spectrum, c) marginal Hilbert spectrum for fault 6 condition.

Table 1. Summary of results of Hilbert-Huang spectrum for self-aligning bearing.

Condition of bearing	Amplitude [m/s^2]	Frequency [Hz]
Healthy bearing	0.037	23.51
Fault 1	0.2473	140.3
Fault 2	0.4217	140.2
Fault 3	0.0610	8.223
Fault 4	0.1331	48.09
Fault 5	0.4551	48.03
Fault 6	0.5699	97.94

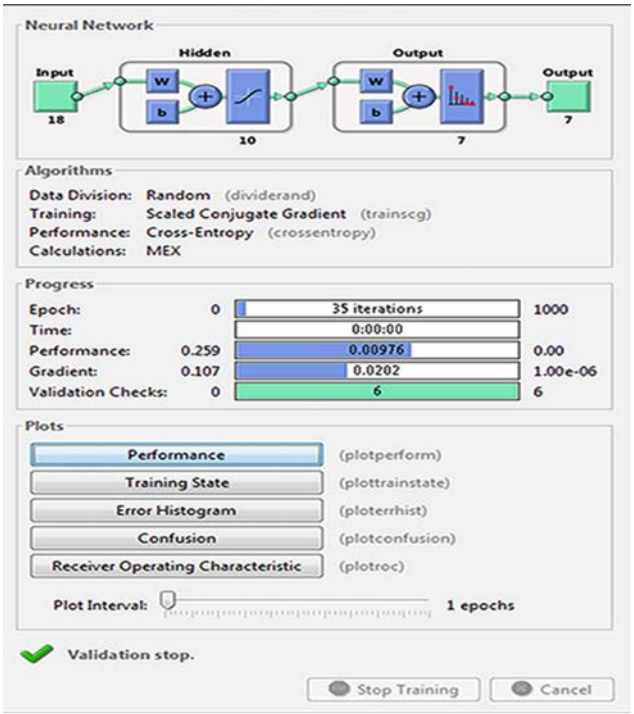

Fig. 11. ANN data.

The various ANN parameters obtained were as follows.

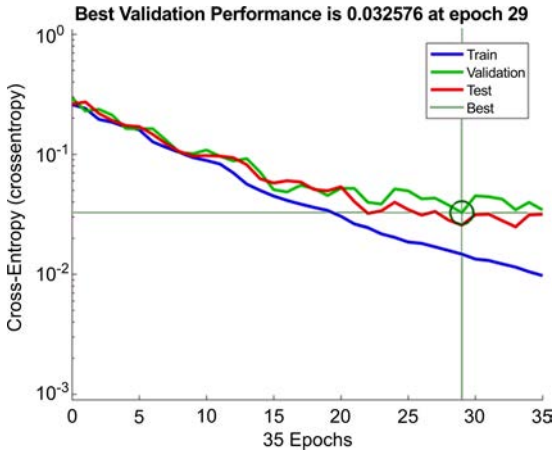

Fig. 12. Performance diagram.

Performance diagram shows how the network error drops. Here cross-entropy error function is used for validation. Blue line shows decreasing error in training data. The green line shows validation error. Training stops when validation error decreases. The red line shows error in the test data. From the graph it is evident that the best validation error is at epoch 29.

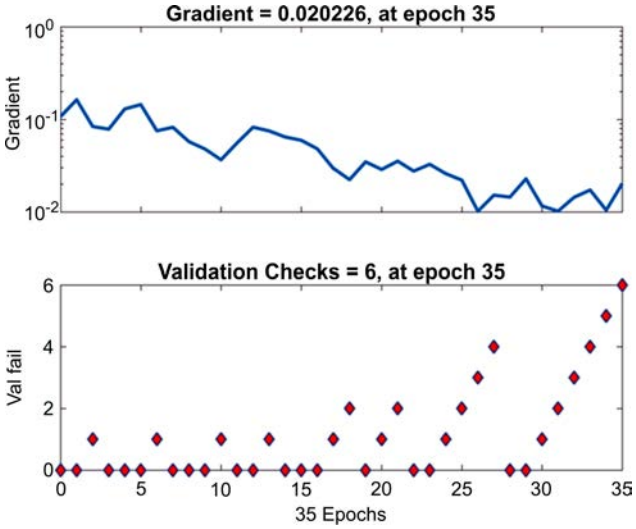

Fig. 13. Training state performance.

From the graph it is evident that the learning algorithm sees the whole data set for 35 times. A total of 6 validation checks are done by the neural network. The graph shows the validation failure at various epochs.

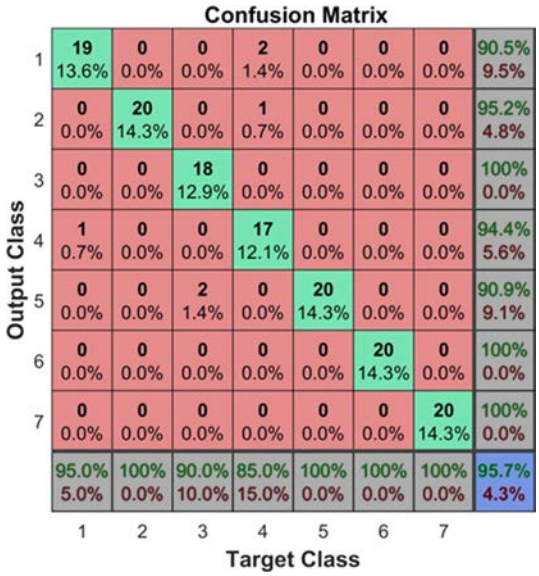

Fig. 14. Confusion matrix summary.

Receiver operating characteristic (ROC) shows the performance of neural network. For a good performance, area under true positive rate should be bigger and it should not cross the false positive rate. Thus,

from the above figure, the method employed can be concluded as good.

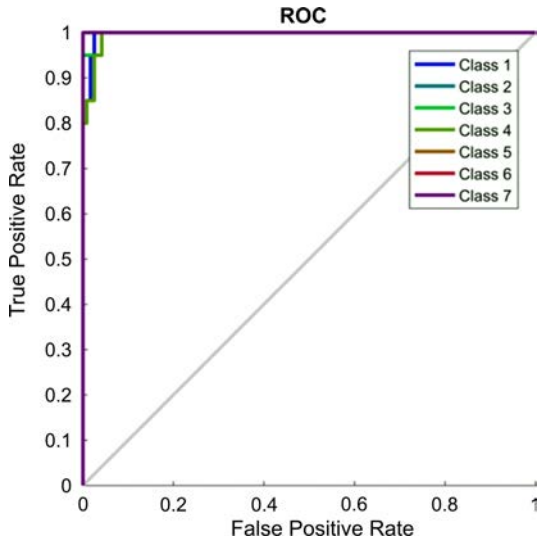

Fig. 15. ROC plots.

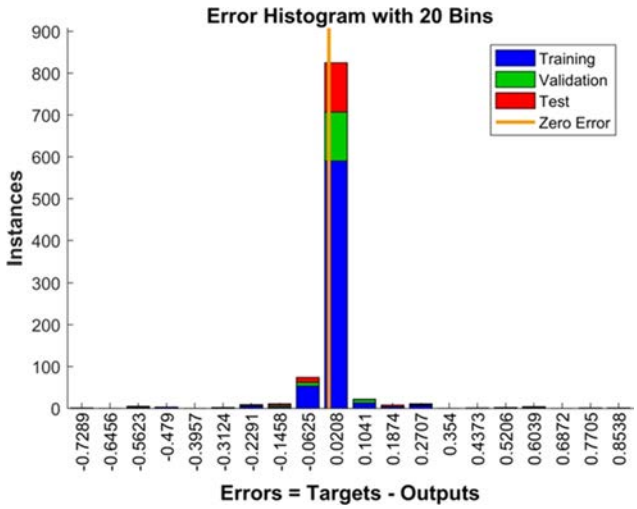

Fig. 16. Error histogram.

The error histogram is done by dividing it into 20 bins. In the graph the errors are near to zero. This also implies the success of the neural network.

4.10. Automatic fault classification using deep neural networks (DNN)

A deep neural network was realised for various fault cases of the taper roller bearing using autoencoders. Two autoencoders and a softmax layer were stacked one after the other to get the neural network. All the performance characteristics were plotted for this neural network. As the number of hidden neuron layers was increased in the deep network, the efficiency increased from 90.8% to 100%. This is highlighted by the confusion matrix. The ROC plot for the neural network also matched with the ideal plot. The DNN parameters as well as various performance plots are shown below.

Due to the increased complexity of the DNN method, an increased number of iterations have been performed on the data. Scaled conjugate gradient algorithm was used for network training while cross entropy technique was used for measurement the performance. In the confusion matrix, the output class refers to the actual output produced, while the target class refers to the ideal output that was expected. Here, an accuracy of 100% was obtained, which meant all the defects were correctly classified. This is due to the ability of DNN to correctly distinguish even the smallest of changes in the feature pattern. The receiver operating characteristics graph also gives an ideal plot in this case.

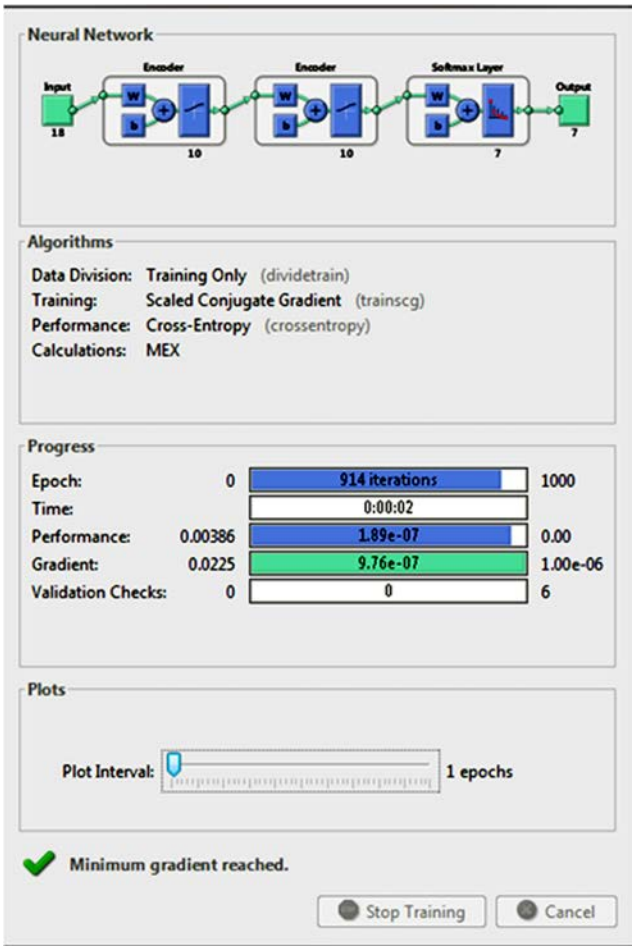

Fig. 17. DNN parameters.

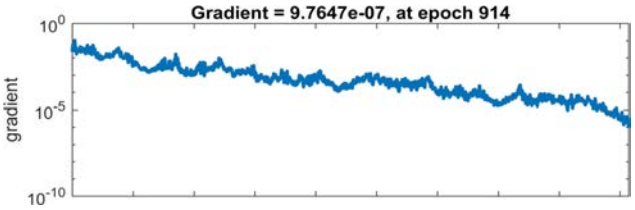

Fig. 18. Training state performance.

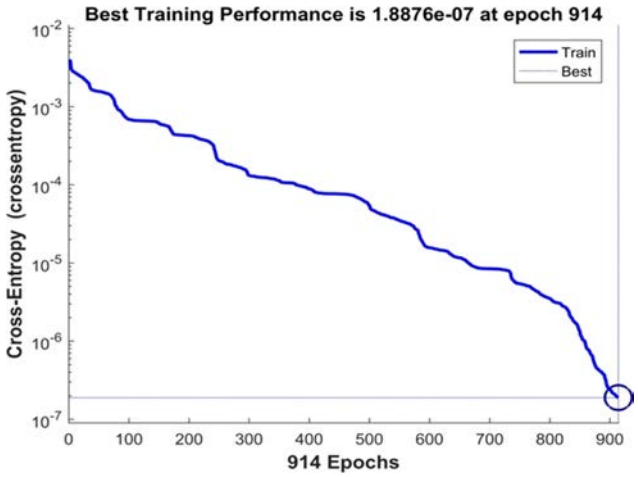

Fig. 19. Performance plot.

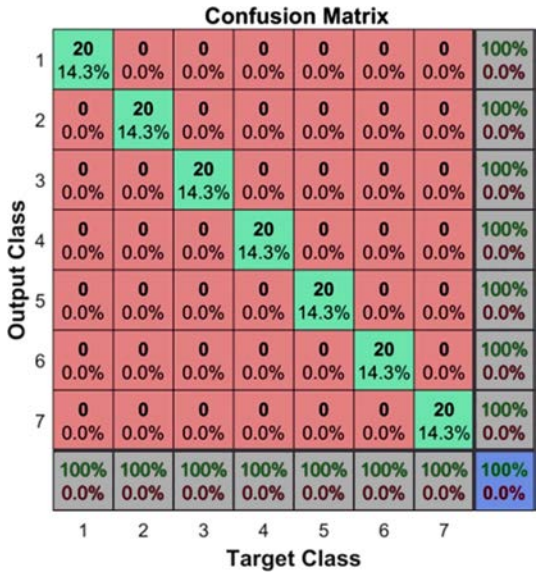

Fig. 20. Confusion matrix.

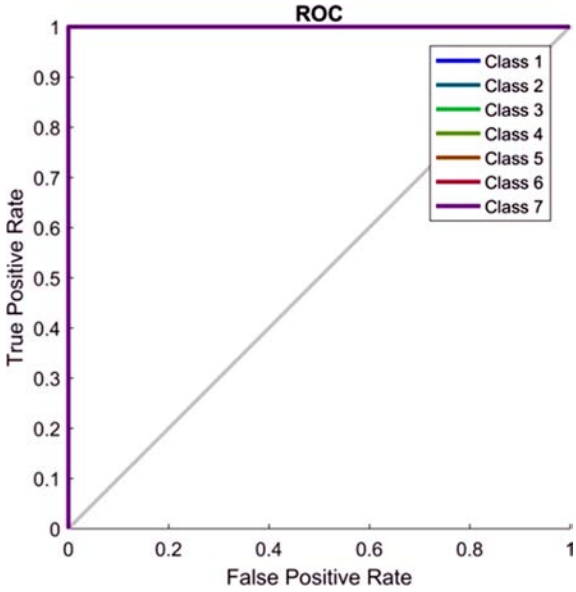

Fig. 21. ROC plot.

5. Conclusion

In this study, empirical mode decomposition has been implemented along with Hilbert Huang transform on the collected vibration data for self-aligning roller bearing. Each instantaneous mode frequency obtained was subjected to Hilbert Huang transform to obtain the corresponding instantaneous frequencies. This is followed by the marginal Hilbert spectrum which produces the frequency spikes at various fault conditions. This method is able to give more precise results as compared to the conventional fast Fourier transform and wavelet transforms. One advantage lies in the ability of this method to process non-linear and non stationary signals. Another advantage is the capability to monitor real time data from bearing which helps to predict defects before failure, hence improving the running time of machines. The major advantage of the empirical mode decomposition lies in the fact that various frequency ranges can be analysed by this method to pin point the fault. This proves helpful in various industries where a large amount of vibration data, maybe for days, needs to be analysed.

The study also highlights the advantages of using deep neural networks over Artificial neural networks. Deep neural networks are widely utilised in image classification and, therefore, the method can scrutinise even minor changes that occur in feature extraction and still produce near accurate results. So, in an industry where the number of faults under consideration is huge, it is preferable to use a deep network which can accurately predict the fault, no matter how minute the difference in vibration data is. However, it is to be noted that the number of iterations involved in deep learning algorithms is very high compared to the artificial neural networks resulting in a higher processing time for the data.

References

1. Ali J.B., Fnaiech N., Saidi L., Chebel-Morello B., Fnaiech F. (2015), *Application of empirical mode decomposition and artificial neural network for automatic bearing fault diagnosis based on vibration signals*, Applied Acoustics, **89**, 16–27, https://doi.org/10.1016/j.apacoust.2014.08.016.
2. Boashash B. (1992a), *Estimating and interpreting the instantaneous frequency of a signal. I. Fundamentals*, Proceedings of the IEEE, **80**, 4, 520–538, doi: 10.1109/5.135376.
3. Boashash B. (1992b), *Estimating and interpreting the instantaneous frequency of a signal. II. Algorithms and applications*, Proceedings of the IEEE, **80**, 4, 540–568, doi: 10.1109/5.135378.
4. Chen Z., Deng S., Chen X., Li C., Sanchez R.-V., Qin H. (2017), *Deep neural networks based rolling bearing fault diagnosis*, Microelectronics Reliability, **75**, 327–333, doi: 10.1016/j.microrel.2017.03.006.

5. Feng Z., Ma H., Zuo M.J. (2016), *Amplitude and frequency demodulation analysis for fault diagnosis of planet bearings*, Journal of Sound and Vibration, **382**, 395–412.
6. Gan M., Wang C. (2016), *Construction of hierarchical diagnosis network based on deep learning and its application in the fault pattern recognition of rolling element bearings*,Mechanical Systems and Signal Processing, **72–73**, 92–104.
7. Huang N.E., Shen Z., Long S.R. (1999), *A new view of nonlinear water waves: The Hilbert Spectrum*, Annual Reviews of Fluid Mechanics, **31**, 1, 417–457.
8. Huang N.E., Shen Z., Long S.R., Wu M.C., Shih H.H., Zheng Q., Yen N.-C., Tung C.C., Liu H.H. (1998), *The empirical mode decomposition and the Hilbert Spectrum for non-linear and non-stationary time series analysis*, Proceedings of the Royal Society of London, Series A: Mathematical, Physical and Engineering Sciences, **454**, 903–995, doi: 10.1098/rspa.1998.0193.
9. Ibrahim A., Guillet F., El Badaoui M., Bonnardot F. (2008), *Techniques to estimate the instantaneous frequency with an aim of diagnosis of induction machines faults*, [in:] Proceedings of 34th Annual Conference of IEEE Industrial Electronics, IECON 2008, Orlando, FL, pp. 391–396.
10. Jia F., Lei YL., Lin J., Zhou X., Lu N. (2016), *Deep neural networks: a promising tool for fault characteristic mining intelligent diagnosis of rotating data with massive data*, Mechanical Systems and Signal Processing, **72–73**, 303–315, doi: 10.1016/j.ymssp.2015.10.025.
11. Kim T.-W., Valdés J.B. (2003), *Nonlinear model for drought forecasting based on a conjunction of wavelet transforms and neural networks*, Journal of Hydrologic Engineering, **8**, 6, 319–328, doi: 10.1061/(ASCE)1084-0699(2003)8:6(319).
12. Rato R.T., Ortigueira M.D., Batista A.G. (2008), *On the HHT, its problems and some solutions*, Mechanical Systems and Signal Processing, **22**, 6, 1374–1394.
13. Samanta B., Al-Balushi K. R., Al-Araimi S.A. (2003), *Artificial neural networks and support vector machines with genetic algorithm for bearing fault detection*, Engineering Applications of Artificial Intelligence, **16**, 7–8, 657-665.
14. Saridakis K.M., Nikolakopoulos P.G., Papadopoulos C.A., Dentsoras A.J. (2008), *Fault diagnosis of journal bearings based on artificial neural networks and measurements of bearing performance*, [in:] Proceedings of the Ninth International Conference on Computational Structures Technology, B.H.V. Topping, M. Papadrakakis [Eds.], Civil-Comp Press, Stirlingshire, UK, Paper 118, 2008, doi: 10.4203/ccp.88.118.
15. Vyas N.S., Satishkumar D. (2001), *Artificial Neural Network Design for fault identification in a rotor bearing system*, Mechanism and Machine Theory, **36**, 2, 157–175.
16. Wu T.Y., Lai C.H., Liu D.C. (2016), *Defect diagnosis of roller bearings using instantaneous frequency normalisation under fluctuant rotating speed*, Journal of Mechanical Science and Technology, **30**, 3, 1037–1048.
17. Yang W.-X. (2008), *Interpretation of mechanical signals using an improved Hilbert-Huang transform*, Mechanical Systems and Signal Processing, **22**, 5, 1061–1071.